ReaxFF-based molecular dynamics study of bio-derived polycyclic alkanes as potential alternative jet fuels

Hyunguk Kwon [a,†], Aditya Lele [b,†], Junqing Zhu [c], Charles S. McEnally [c], Lisa D. Pfefferle [c], Yuan Xuan [b] and Adri C.T. van Duin [a,b,*]

[a] *Department of Chemical Engineering, The Pennsylvania State University, University Park, PA 16802, USA*

[b] *Department of Mechanical Engineering, The Pennsylvania State University, University Park, PA 16802, USA*

[c] *Department of Chemical and Environmental Engineering, Yale University, New Haven, CT 06520, USA*

[*] *Corresponding authors: acv13@psu.edu (A.C.T. van Duin)*

[†] *Authors contributed equally.*

Accepted for publication in Fuel

Abstract

This work investigates the initial stages of the pyrolysis of HtH-1 ($C_{18}H_{32}$; 2,2,7,7,8a,8b-hexamethyl-dodecahydrobiphenylene) and HtH-2 ($C_{18}H_{34}$; 1,1′,3,3,3′,3′-hexamethyl-1,1′-bi(cyclohexane)), which are bio-derived polycyclic alkanes and potential jet fuels, using ReaxFF force field based molecular dynamics (MD) simulations. Global Arrhenius parameters, such as activation energies and pre-exponential factors, are calculated and used to analyze the overall decomposition kinetics of the fuels. HtH-1 decomposes faster than HtH-2 at the same temperature and density conditions, and they have a faster decomposition rate compared to some existing jet-fuels, such as JP-10. A systematic reaction analysis framework developed in this work is applied to determine a temperature-dependent decomposition mechanism. At lower temperature, the central C-C bond connecting the two cyclohexane rings is dominantly broken in both HtH-1 and HtH-2. However, C-CH_3 bond breaking becomes dominant with increasing temperature due to the large increase in entropy during this reaction. Major products from HtH-1 are C_5H_8 and C_4H_8, and those from HtH-2 are C_4H_8 and C_2H_4. The major products predict that HtH-1 has a higher sooting tendency than HtH-2, which is consistent with measurements. The impact of HtH-2 on the pyrolysis of HtH-1 is also investigated in their binary mixtures. HtH-1 and HtH-2 decompose by unimolecular reactions, and they rarely interact with each other during the pyrolysis of the mixtures. This work demonstrates that ReaxFF can be used to investigate pyrolysis and combustion chemistry of existing or future fuels and to contribute to the development of their chemical kinetic models without any *a priori* input and chemical intuition.

Keywords: Molecular dynamics, ReaxFF reactive force field, Pyrolysis, Bio-derived jet fuel

1. Introduction

For ground transportation, there is an ongoing push to replace conventional vehicles powered by internal combustion engines with electric vehicles, due to the environmental benefits. However, such a strategy is not yet practical for aviation applications, since electric aircraft still have much more limited payload and flight range compared to conventional jets [1]. Therefore, there is considerable interest in utilizing fuels derived from biomass for future sustainable aviation applications which can alleviate environmental concerns from traditional fuels, such as global warming and pollutant emissions [2-6].

High energy density is an essential property required for aviation fuels to ensure the range and payload of volume-limited air vehicles [1, 7]. To afford high energy density, for example, current rocket and jet fuels, such as RP-1 and JP-10, contain highly strained multi-cyclic hydrocarbons [8]. In response, many researchers have made an effort to synthesize energy-dense bio-fuels containing polycyclic hydrocarbons from a variety of biomass-derived platform chemicals [7]. For example, isophorone, which is a α, β-unsaturated cyclic ketone, has been regarded as a promising feedstock [9-12]. Related literature shows that the hydrodeoxygenation of isophorone can produce high energy density fuels, such as 1,1,3-trimethylcyclohexane [9] and dimers of isophorone [10]. Substituted cyclohexanes derived from isophorone and furanic aldehydes have been also shown as high energy density fuels [11]. In addition, a recent experimental study reported a new synthesis route of promising aviation fuels from upgrading bio-acetone via isophorone [12]. A cyclobutene dione was produced from isophorone, and hydrodeoxygenation of the dione yielded a mixture of head-to-head polycyclic alkanes (HtH-1 and HtH-2; see structures in Figure 1). The energy density of the mixture (38.0 MJ L^{-1}) is significantly higher than the energy density of Jet-A (34.0 MJ L^{-1}) [12].

To use the proposed polycyclic hydrocarbon fuels for aviation applications, it is necessary to understand their combustion chemistry, which could help to predict important

combustion properties, including ignition, extinction, heat release, and formation of potential pollutants. There has been extensive experimental and theoretical literature on pyrolysis and combustion behaviors of monocyclic alkanes, such as cyclohexane [13], methylcyclohexane [14], ethylcyclohexane [15], *n*-propylcyclohexane, 1,3,5-triisopropylcyclohexane [16], and *n*-butylcyclohexane [17], and representative polycyclic alkanes, such as decalin [18, 19] and JP-10 [20-23]. However, there have been no studies of compounds such as HtH-1 that contain four-membered carbon rings fused with other rings. There are also very few studies of compounds like HtH-2 that contain cycloalkyl rings joined by a carbon-carbon single bond. Yue *et al.* studied the thermal decomposition kinetics of 1,1′-bicyclohexyl, which has two separated cyclohexyl rings, in a batch-type reactor and carried out quantum calculations to explain the product distribution [24]. They found that the major initial product of 1,1′-bicyclohexyl is cyclohexyl radical due to the relatively low energy of the C−C bond connecting the two cyclohexyl rings. Despite this previous study, there is still a significant lack of understanding of decomposition mechanism and kinetics of HtH polycyclic alkanes.

Understanding the reaction dynamics of a fuel species typically involves coordinated efforts involving combustion kinetics-based experiments as well as quantum mechanics (QM) calculations. QM-based methods have been extensively used to investigate combustion and pyrolysis chemistry of fuels by calculating reaction energies and activation barriers [25]. The kinetic parameters calculated from QM methods also have greatly contributed to the development of detailed chemical kinetic models required to simulate practical combustion devices [25]. However, the methods have limitations in system size and time scale due to the high cost for computation. Moreover, QM calculations require that the reactions of interest be provided *a priori*, and the reaction pathways suggested can depend on the user's chemical intuition. This greatly increases the efforts required to investigate the reaction chemistry of the fuel of interest, especially for fuels which do not show close structural proximity with existing,

well studied fuels such as *n*-alkanes, alkenes, etc. This makes it challenging to deal with chemical processes of complex and large fuel molecules, such as polycyclic alkanes.

As an alternative to QM, ReaxFF reactive force field based molecular dynamics (MD) can be a powerful computational tool to simulate complex reactive systems [26-28]. The ReaxFF reactive force field is mainly trained against QM data and the ReaxFF methodology describes chemically reactive events through the interatomic potential within a bond-order formalism, thus describing bond formation and breaking without expensive QM calculations. Since ReaxFF requires significantly lower computational cost than QM, it can simulate reaction processes over longer time and larger scales. Additionally, ReaxFF does not require any user intuition for possible reaction processes beyond its initial training, thus enabling it to simulate complex reactive systems, such as combustion. This greatly facilitates the investigation of fuel chemistry.

In the present work, we investigate, using ReaxFF-MD methods, the high-temperature pyrolysis of the HtH polycyclic alkanes recently synthesized experimentally by Ryan *et al.* [12]. The synthesis method led to a mixture of 91.2 % of cyclobutane moiety ($C_{18}H_{32}$; 2,2,7,7,8a,8b-hexamethyl-dodecahydrobiphenylene, termed HtH-1), as the desired product, and 8.8 % of an impurity ($C_{18}H_{34}$; 1,1′,3,3,3′,3′-hexamethyl-1,1′-bi(cyclohexane), termed HtH-2), which is a cyclobutane ring-opening product (see structures in Figure 1). This work examines the pyrolysis of both these compounds. As mentioned earlier, these compounds with high energy density are potential fuels for the aviation industry, however, neither experimental nor theoretical studies on combustion chemistry of these compounds have yet been reported. The specific objectives of the present paper are three-fold. First, this work seeks to investigate fuel decomposition kinetics in pyrolysis of HtH-1 and HtH-2. Arrhenius parameters for fuel decomposition are calculated from the ReaxFF simulations and are compared with those of existing jet-fuel components. Second, we aim to elucidate the initial decomposition mechanism,

and identify the product distribution resulting from the decomposition. Our third goal is to examine the pyrolysis behavior in mixtures of HtH-1 and HtH-2 to analyze the impact of the impurity (HtH-2) on the pyrolysis of the desired product (HtH-1). The results reported in this work provide important atomistic insights on the pyrolysis of HtH polycyclic alkanes, a candidate fuel for aviation applications.

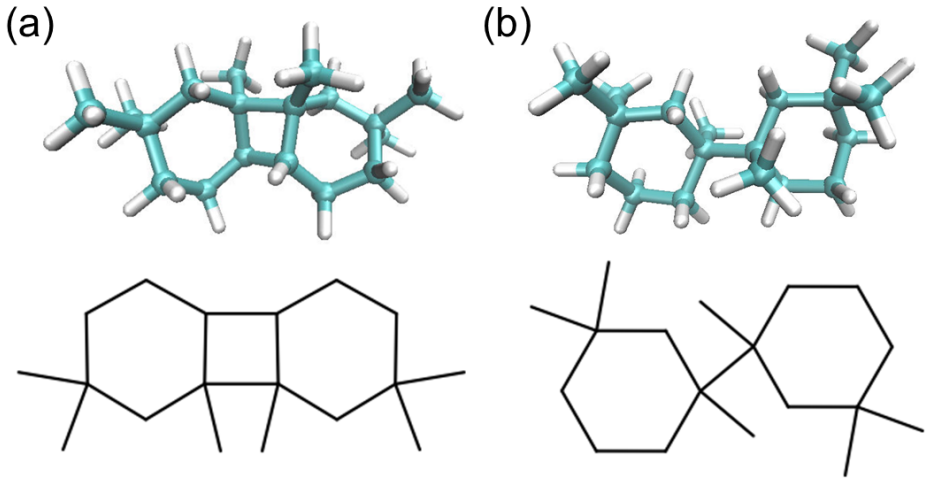

Fig. 1. Molecular structure of (a) HtH-1 ($C_{18}H_{32}$; 2,2,7,7,8a,8b-hexamethyl-dodecahydrobiphenylene) and (b) HtH-2 ($C_{18}H_{34}$; 1,1′,3,3,3′,3′-hexamethyl-1,1′-bi(cyclohexane)). Cyan and white spheres represent carbon and hydrogen atoms respectively.

2. Simulation details

2. 1. ReaxFF reactive force field method

The ReaxFF reactive force field based molecular dynamics method allows bond formation and bond breaking during simulation, which enables us to describe complex reactive systems [26-28]. Briefly, in the ReaxFF methods, reactive events are described through a bond-order concept, where the bond order is calculated directly from interatomic distance using an empirical formula that contains the single, double, and triple bond order contributions. The bond order is updated at every iteration, which allows ReaxFF to describe bond formation and

bond breaking. Non-bonded interactions, such as van der Waals and Coulomb, are calculated between every pair of atoms and they are independent from the bonded-interactions. Atomic charges are calculated using a geometry-dependent charge calculation scheme, Electronegative Equalization Method (EEM) [29]. The ReaxFF methods calculate the energy on each atom using the following equation.

$$E_{system} = E_{bond} + E_{over} + E_{under} + E_{lp} + E_{val} + E_{tor} + E_{vdWaals} + E_{Coulomb}. \quad (1)$$

In the above equation, E_{bond} (bond energy), E_{over} (over-coordination penalty energy), E_{under} (under-coordination penalty energy), E_{lp} (lone pair energy), E_{val} (valence angle energy), E_{tor} (torsion angle energy) are bond-order-dependent terms. $E_{vdWaals}$ (van der Waals energy) and $E_{Coulomb}$ (Coulomb energy) are non-bonded terms. A more detailed description can be found in previous ReaxFF-related papers [26-28].

Chenoweth *et al.* developed the first version of the combustion force field (CHO-2008) [27], and it has been extensively applied to pyrolysis and combustion studies of single component fuels, such as *n*-heptane [30], *n*-dodecane [31], toluene [32], 1,6-dicyclopropane-2,4-hexyne [33], and JP-10 [27] as well as hydrocarbon mixtures, such as RP-1 [34] and RP-3 [35]. Initial oxidation reaction of a 24-component model bio-oil was also studied [36] using the DREIDING force field [37]. Recently a new version of the CHO-2008 force field has been developed by Ashraf *et al.* (CHO-2016) [38] to improve upon the C1 chemistry. The recent combustion force field has also shown good capability to describe the pyrolysis and the combustion of single component fuels [22, 38-41] or fuel mixtures [22, 42, 43]. In the current work, the CHO-2016 force field is used for all the simulations.

2. 2. ReaxFF MD simulations

In this work, we investigate the pyrolysis of HtH-1, HtH-2, and mixtures of HtH-1 and HtH-2. For single component systems, 40 energy-minimized molecules of each type are placed

in a cubic box with a dimension required to produce the desired densities (0.1, 0.2, and 0.3 kg/dm^3). For mixture systems, the total number of fuel molecules is kept at 40, but the mixture composition is changed by changing the amount of HtH-1 and HtH-2 molecules. We define the ratio between the number of HtH-1 molecules and the total number of fuel molecules as α, and this study considers three mixtures with $\alpha = 0.9$, 0.7, and 0.5 to assess the effects of the impurity (HtH-2). As demonstrated in earlier ReaxFF studies [22, 27, 38], the selected number of fuel molecules and system density are sufficient to investigate the reaction channels of hydrocarbon initial pyrolysis and to estimate reasonable Arrhenius parameters.

For pyrolysis studies using ReaxFF, a well-established simulation framework is followed here [22, 27, 38]. A system is prepared by randomly placing the desired number of fuel molecules in their energy minimized structures in a periodic simulation box. The prepared system is then equilibrated through NVT-MD simulations at 1500 K. Here, NVT-MD simulation indicates that the number of atoms (N), volume (V), and temperature (T) are kept constant during the simulations. The total time for the equilibrium simulations (2.5 ps) is short enough that no fuel molecules thermally decompose at the chosen temperature. The Berendsen thermostat [44] with a temperature damping constant of 100 fs is used to control the temperature. Once the system is equilibrated, NVT-MD simulations are performed at different temperatures ranging from 1500 K to 3000 K using a time step size of 0.1 fs. To get statistically meaningful results, the simulations are performed with 10 independent starting configurations at a given condition, and the results are ensemble-averaged.

In general, reaction events happen less frequently at lower temperatures for a given simulation time, which makes it difficult to access low temperatures with regular MD simulations due to the high computational expense. For NVT-MD simulations at 1500 K, therefore, the control variable driven hyper-dynamics (CVHD) method [45, 46] is used to accelerate the simulation. The CVHD method applies a biased potential in the potential energy

surface of a system, filling energy minima and consequently lowering the reaction barrier. The method has shown good agreement with experiments and existing chemical kinetic models for pyrolysis and oxidation of hydrocarbons [22, 45, 46]. At very high simulation temperatures (e.g., 3000 K), simulations with a smaller time step size of 0.05 fs are also performed and shown to give almost identical results, which confirms that a time step size of 0.1 fs provides the appropriate temporal resolution. These comparisons can be found in the supplementary material (S1). The reaction dynamics of hydrogen atoms are typically very fast, and hence it is essential to verify the temporal resolution especially for high temperature pyrolysis of hydrocarbons.

2. 3. Potential energy surface calculations using ReaxFF

Along with the pyrolysis reaction mechanisms obtained using the ReaxFF-MD simulations, we also report free energies for the reactant, transition state, and product complexes to get further insight into the reaction kinetics and its temperature dependence. The decomposition reactions are first identified using an in-house reaction analysis code based on the results of NVT-simulations. The reaction dynamics of these reactions including the order and location of bond breaking is traced using the ReaxFF-MD simulation trajectories. This information is then utilized in ReaxAMS modelling suite, which is a part of the ADF software [47], to obtain the potential energy surface (PES) for the reactions. The transition state geometries are identified by the presence of one imaginary frequency and further confirmed by performing intrinsic reaction coordinate (IRC) calculations to ensure the correct transition state is found for the corresponding reactant and product complexes. More details and an example study for a sample hydrocarbon, cyclohexane [48], can be found in the supplementary material (S2).

2. 4. Quantum mechanical calculation

Density functional theory (DFT) calculations are performed for HtH-1 and HtH-2 to calculate bond dissociation energy (BDE) using the Jaguar software package [49]. All geometries are calculated using a hybrid method employing Becke's three-parameters approach, B3LYP [50], and the 6-311G** basis sets [51], which were also used in the development of the CHO-2016 force field [38].

3. Results and discussions

3. 1. Analysis of bond dissociation energy (BDE)

BDE, the energy required to break a chemical bond, is first calculated to provide insight into the thermal decomposition via unimolecular reactions. Table 1 lists all the BDEs relevant to the most important decomposition reactions identified by ReaxFF using both ReaxFF and DFT. Additionally, various C-H BDEs are also calculated for reference. The agreement between ReaxFF and DFT BDE results is in the acceptable range, similar to those reported in previous studies [38]. Note that this ReaxFF parameter set was trained to reproduce experimental atomization energies for hydrocarbons, which resulted in a systematically lower BDE energy compared to DFT methods [38], since DFT methods tend to over-estimate atomization energies [52, 53].

As expected, the C-C bonds have smaller BDEs than the C-H bonds, which implies that thermal decomposition of the fuels should primarily involve C-C bond fissions. In HtH-1, the connected cyclohexyl rings make a highly strained cyclobutyl structure in the middle. This makes it easy to break the C^g-C^j bond composed of two quaternary carbon atoms, and hence it has exceptionally low BDE. This implies that C^g-C^j bond fission is likely to initiate thermal decomposition of HtH-1, which will be confirmed in the next section. In comparison, the C^a-C^c, C^b-C^c and C^g-C^i bonds have much higher BDEs.

In HtH-2, ReaxFF and DFT results show that the C^g-C^j bond has the lowest BDE, since the bond is formed between two quaternary carbon atoms. However, the BDE for the C^g-C^j bond is only around 16 kcal/mol less than that for C^g-C^i in HtH-2, compared to a much larger difference of 66.3 kcal/mol in HtH-1. ReaxFF predicts similar BDEs (~60.0 kcal/mol) for the C^a-C^c, C^b-C^c and C^g-C^i bonds, although DFT predicts that the C^a-C^c and (78.1 kcal/mol) C^b-C^c (76.9 kcal/mol) bonds have a slightly larger BDE than the C^g-C^i bond (69.4 kcal/mol). In general though, the DFT and ReaxFF results are very similar, which demonstrates that the CHO-2016 force field employed in this study can be used to describe the complex polycyclic compounds, HtH-1 and HtH-2.

Table 1. Bond dissociation energies (BDE) calculated for HtH-1 and HtH-2 using ReaxFF and DFT. The values are reported in kcal/mol. Carbon "a" is defined as being out-of-the-plane in the same direction as carbon "i".

Bond	HtH-1 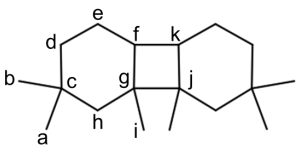		HtH-2 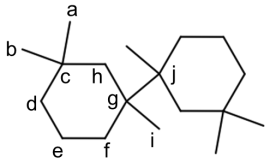	
	ReaxFF	DFT	ReaxFF	DFT
C^a-C^c	65.5	76.7	60.0	78.1
C^b-C^c	65.4	76.7	60.0	76.9
C^g-C^i	67.3	78.7	59.7	69.4
C^g-C^j	1.0	10.8	43.7	49.0
C^a-H	98.0	105.3	97.8	106.8
C^d-H	86.8	102.7	87.0	102.5
C^e-H	81.3	99.9	82.9	101.4
C^f-H	77.3	101.2	81.5	100.6
C^h-H	83.2	97.7	83.5	98.7

C^i-H	92.3	102.8	92.6	102.2

3. 2. Pyrolysis in single component systems

3. 2. 1. Fuel decomposition rates

Gas-phase reactivity at combustion temperatures is important for determining the location of combustion events and combustion efficiency in practical combustion devices. Therefore, we investigate the thermal decomposition kinetics of HtH-1 and HtH-2 in this section. The fuel decomposition rates extracted from the NVT-MD simulations performed over a wide temperature range (1500-3000 K) are used to obtain global Arrhenius parameters for each fuel investigated assuming irreversible unimolecular fuel decomposition. To calculate the Arrhenius parameters, a well-established method widely used in previous ReaxFF papers [22, 31-33, 38, 54] is employed. The rate constant is determined at each temperature using the following integrated first order-rate law equation,

$$\ln(N_0) - \ln(N_t) = \mathrm{k}t, \quad (2)$$

where N_0 is the initial number of molecules, N_t is the number of molecules at any time t, and k is the rate constant. The time evolution of the number of fuel molecules is shown in the supplementary material (S3). $\ln(N_0) - \ln(N_t)$ computed using the ReaxFF simulation results is found to vary linearly with time, which suggests that the first-order irreversible unimolecular fuel decomposition is a reasonable approximation. The time required for 50% fuel consumption is used to calculate the rate constants (k) at 1800-3000 K. Since a very long simulation time is required to consume 50% of the fuel at 1500 K even using the CVHD method, the rate constant at 1500 K is calculated with the time required for 25% fuel consumption. The Arrhenius equation

$$\mathrm{k} = Ae^{\frac{-E_a}{RT}} \quad (3)$$

281 is then fit to these rates to obtain the pre-exponential factor (A) and the activation energy (E_a)
282 values where R is the universal gas constant. The rate constants are determined using 50% (or
283 25%) fuel consumption to make sure that the fuel decomposition stays linear with respect to
284 temperature or in the simple Arrhenius form as specified above. The calculations are performed
285 at 3 different densities (0.1 kg/dm^3, 0.2 kg/dm^3, and 0.3 kg/dm^3).

286 Figure 2 shows the logarithm of reaction rate constant plotted against the inverse of
287 temperature. It is observed that first-order kinetics fit very well to the Arrhenius equation above.
288 It also demonstrates that the methodology we are using which averages over 10 independent
289 ReaxFF simulations with 40 fuel molecules in each simulation is able to produce reaction rates
290 with minimal statistical uncertainties. E_a and A at 0.2 kg/dm^3 extracted from Fig. 2 are 27.97
291 kcal/mol and 2.51×10^{13} 1/s for HtH-1 and 49.20 kcal/mol and 5.99×10^{14} for HtH-2. System
292 density doesn't affect the first-order kinetics of the fuels significantly, as shown in Fig. 2 and
293 Table 2. Although the pre-exponential factor is about one order of magnitude higher in HtH-2
294 than HtH-1, HtH-1 has higher decomposition rates due to the significantly low activation
295 energy.

296 As the fuels investigated in the current study were only successfully synthesized
297 recently [12], there is a lack of any kind of experimental data for validation. To compare the
298 reactivity of HtH-1 and HtH-2 with existing fuels, therefore, Table 2 also lists the Arrhenius
299 parameters calculated for other jet fuels or jet fuel surrogates from previous ReaxFF studies
300 [22, 54], which showed excellent agreement with their respective experimental data. Both HtH-
301 1 and HtH-2 have higher reactivity compared to the *n*-alkane, *iso*-alkane and aromatic
302 components representative of the jet fuel components. HtH-2 has similar reactivity as JP-10
303 (tetrahydrodicyclopentadiene) with its activation energy of decomposition approximately 5
304 kcal/mol lower than JP-10. HtH-1 is clearly the most reactive largely due to the highly strained
305 cyclobutane moiety, which is discussed later.

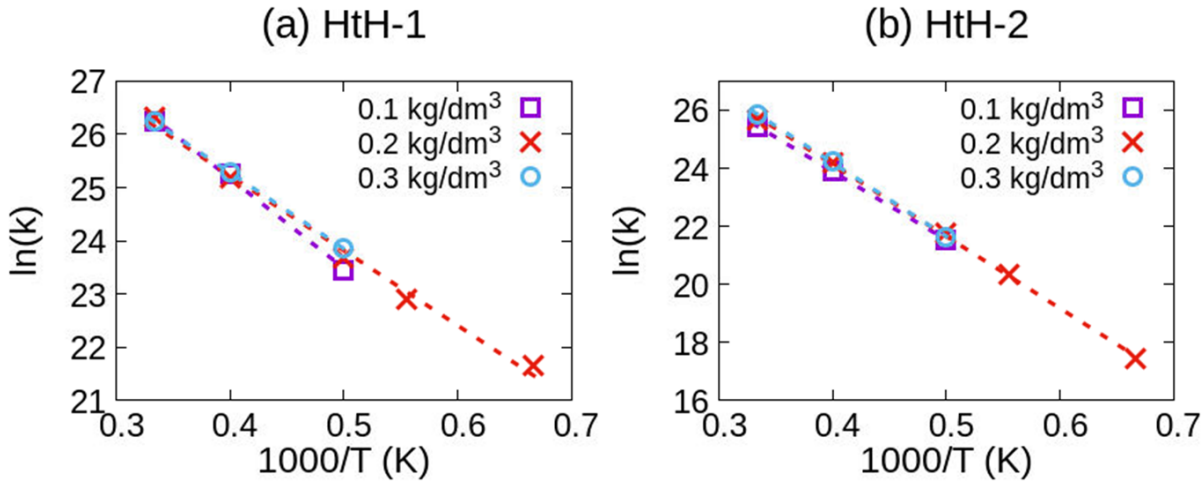

Fig. 2. The logarithm of the global reaction rate constant (ln(k)) plotted against the inverse of temperature (1000/T) in the thermal decomposition of (a) HtH-1 and (b) HtH-2 with system densities of 0.1 kg/dm^3, 0.2 kg/dm^3, and 0.3 kg/dm^3.

Table 2. Fitted Arrhenius parameters for the thermal decomposition of HtH-1 and HtH-2. The reaction rates (k) calculated based on these parameters at 2000 K using the Arrhenius equation are shown in the last column. The parameters for other fuel components are obtained from previous ReaxFF papers.

Molecule	Density (kg/dm^3)	E_a (kcal/mol)	A (1/s)	k_{2000K} (s)
HtH-1	0.1	31.92	6.75×10^{13}	2.19×10^{10}
	0.2	27.97	2.51×10^{13}	2.20×10^{10}
	0.3	28.41	2.90×10^{13}	2.28×10^{10}
HtH-2	0.1	43.92	1.74×10^{14}	2.76×10^{9}
	0.2	49.20	5.99×10^{14}	2.52×10^{9}
	0.3	50.33	7.99×10^{14}	2.53×10^{9}
JP-10 [22]	0.2	54.33	1.56×10^{15}	1.80×10^{9}
n-dodecane [22]	0.2	60.94	9.50×10^{15}	2.08×10^{9}
iso-octane [54]	0.14	60.22	1.23×10^{15}	3.23×10^{8}
toluene [22]	0.2	95.71	2.83×10^{17}	9.82×10^{6}

315 **3. 2. 2. Initial fuel decomposition channels**

316 ReaxFF is well suited for the investigation of fuel decomposition chemistry, especially
317 for fuels with complex molecular structures. A standard framework is proposed in this work
318 and applied to systematically determine the initial fuel decomposition chemistry and its
319 energetics for the two fuels. First, all reaction events that occur during the NVT-MD
320 simulations are identified at every temperature using an in-house reaction analysis code. The
321 in-house code considers that a reaction event occurs when formulaically different chemical
322 species are identified. Such reaction events are identified in each and every simulation, and
323 their occurrence is then averaged over the number of simulations at a given temperature. Table
324 3 shows the important initial reactions identified at different temperatures during the pyrolysis
325 of HtH-1 and HtH-2. It should be noted that these reactions are not necessarily elementary as
326 clarified later. Second, trajectories of the key reactions are visualized and tracked to elucidate
327 the bond breaking sequence in the elementary reactions involved. Third, the information is used
328 to calculate free energies of reactants, TS structures, and products in elementary reactions
329 following the methodology described in Section 2.3. This procedure can provide free energy
330 profiles, as shown in Figs. 3 and 4, and can be used to energetically understand the
331 decomposition mechanism identified by NVT-MD simulations. Considering the lack of
332 significant effects of density on the reactivity of the fuels as shown in Fig. 2, results are shown
333 only for the simulations at 0.2 kg/dm^3 in the following.

334

335 **3. 2. 2. 1. HtH-1 decomposition**

336 **Table 3.** Initial decomposition mechanism of HtH-1 and HtH-2 in the single component
337 systems at different temperatures. Typical statistical error for these results is ± 5 %.

Reactant	Initial Products	Percentage

		1500 K	1800 K	2000 K	2500 K	3000 K
HtH-1 ($C_{18}H_{32}$)	(A1) $C_9H_{16} + C_9H_{16}$	81%	72%	61%	53%	40%
	(A2) $C_{14}H_{24} + C_4H_8$	14%	18%	16%	17%	15%
	(A3) $C_{17}H_{29} + CH_3$	1%	2%	3%	10%	16%
HtH-2 ($C_{18}H_{34}$)	(A4) $C_9H_{17} + C_9H_{17}$	26%	18%	20%	17%	10%
	(A5) $C_{17}H_{31} + CH_3$	19%	26%	25%	37%	36%
	(A6) $C_{12}H_{22} + C_6H_{12}$	16%	11%	16%	12%	11%
	(A7) $C_{14}H_{26} + C_4H_8$	8%	11%	10%	10%	10%

ReaxFF simulations predict that HtH-1 decomposes mainly through 3 different channels (Table 3). As discussed earlier in Section 3.1, the highly strained central cyclobutane moiety is the easiest to break based on the BDE analysis. Consistently, reaction A1 is the primary fuel decomposition pathway at all the temperatures. The reaction A2 seemingly involves the breaking of multiple bonds and results in the formation of $C_{14}H_{24}$ and C_4H_8. Another important pathway is the breaking of the CH_3 groups attached to the rings. Breaking of all the CH_3 groups is grouped together for the comparison purpose. An interesting trend to note here is that the CH_3 breaking only becomes important at higher temperature at the expense of central ring breaking. However, the BDEs alone cannot completely explain this trend.

Therefore, these reactions are further investigated to obtain their energetics following the methodology described in Section 2.3. As mentioned above, the ReaxFF MD simulation trajectories for reactions A1, A2, and A3 are extracted first to identify the bond breaking sequence in each reaction. In reaction A1, as shown in Fig. 3, the central ring breaking in HtH-1 takes place in two steps. First the C-C bond attaching the quaternary C atoms breaks followed by the breaking of the C-C bond attaching the tertiary C atoms. It should be noted that, for verification, the breaking of the tertiary C-C bond followed by the quaternary C-C bond is also investigated, and this reaction sequence is found to be energetically less favorable due to higher

barrier (not shown here). Reaction A2 involves the breaking of the C-C bond part of the cyclohexyl ring followed by ring opening and breaking resulting in C_4H_8 and $C_{14}H_{24}$. A notable feature of the HtH-1 decomposition is that the products of reactions A1 and A2, which account for the majority of fuel decomposition, are stable species rather that radicals. In reaction A3, the CH_3 group attached to C^c atom is found to preferentially dissociate from HtH-1.

To explain the temperature dependence of these reactions, the relative Gibbs free energy (ΔG) diagrams for reactions A1, A2, and A3 at the two extremes of the temperatures investigated (1500 K and 3000 K) are plotted in Fig. 3. Note that the percentages of the A3 reaction in Table 3 result from the breaking of C^a-C^c, C^b-C^c, and C^g-C^i bonds as mentioned above; however, the energy diagram in Fig. 3 only shows the C^a-C^c bond dissociation pathway for simplicity. The reactant is set to have a Gibbs free energy of 0. At 1500 K, reactions A1 and A2 have a similar initial energy barrier. In reaction A2, however, the barrier for the backward reaction is negligible, leading to a significant portion of the first intermediate formed (INT1) to convert back to the reactant. Therefore, despite having similar energy barriers, reaction A1 is strongly favored over reaction A2. Figure 3 also shows that reaction A3 has a quite high reaction barrier, resulting in the negligible occurrence of this reaction at 1500 K. This scenario changes at 3000 K especially for reaction A3. At 3000 K, reaction A3 has the lowest energy barrier due to a huge increase in entropy during the dissociation of CH_3. Hence, the fraction of fuel decomposition through reaction A3 increases significantly compared to that of 1500 K but it is not the most dominant reaction (A1) despite having a smaller barrier due to the much larger reaction energy. The free energy diagrams clearly explain the trends observed in the number of occurrences of the reactions for the decomposition of HtH-1 with temperature.

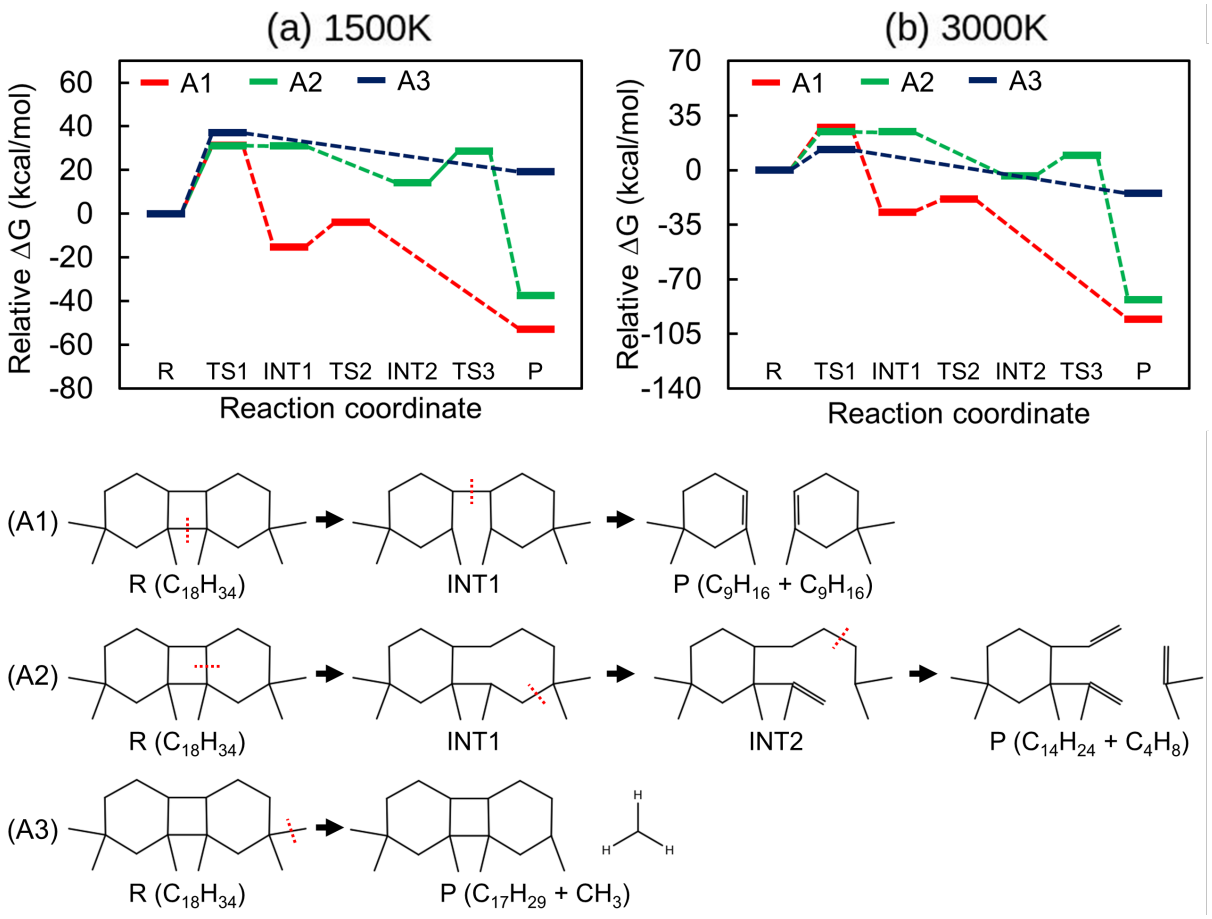

Fig. 3. Gibbs free energy profiles for HtH-1 decomposition reactions A1, A2, and A3 at 1500 K and 3000 K. The reactant (HtH-1) is labeled as "R". The intermediates are labeled as "INT1" and "INT2". The transition states are labeled as "TS1", "TS2", and "TS3". The products are labeled as "P".

3. 2. 2. 2. HtH-2 decomposition

The same analysis is applied to the HtH-2 decomposition reactions. Figure 4 shows the free energy diagrams as well as elementary reaction sequences for reactions A4 and A5 that are the most important reactions in HtH-2 decomposition. Although reaction A5 has three possible pathways via the breaking of C^a-C^c, C^b-C^c, and C^g-C^i bonds, we only show the C^g-C^i bond dissociation pathway in Fig. 4 for simplicity. As shown in Fig. 4, reaction A4 occurs through the breaking of the C^g-C^j bond. Energetically, reaction A4 has a lower barrier at 1500

K while reaction A5 has the lower barrier at 3000 K. Previously, Yue *et al.* reported that the thermal decomposition of 1,1′-bicyclohexyl, structurally similar to HtH-2, is mainly initiated through the dissociation of the C-C bond connecting the two cyclohexyl rings at 683-713 K [24], consistent with our results. The BDEs given in Table 3 indicate that the central C-C bond breaking should be favored over the bond breaking of the C-CH_3 bond. However, a large increase in entropy makes the C-CH_3 bond breaking more favorable at higher temperatures as seen in Fig. 4. This result explains the temperature-dependent initial products observed in the NVT-MD simulations shown in Table 3.

The systematic reaction analysis framework using ReaxFF discussed above provides a reliable way to investigate the fuel decomposition chemistry without any manual intervention and any *a priori* information at a fraction of the computational cost of equivalent QM calculations. This strategy is particularly useful for the current fuels as there are no structural equivalents to them which have been investigated with either QM calculations or experiments.

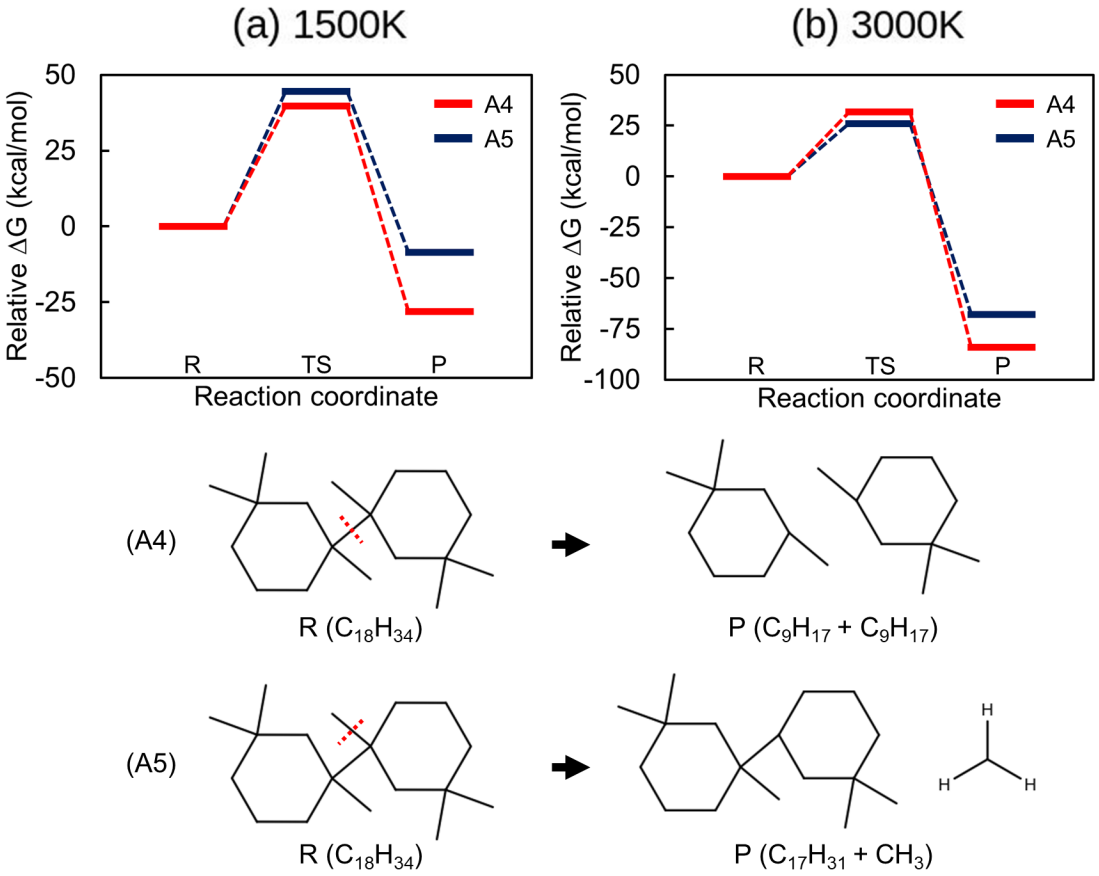

406

407 **Fig. 4.** Gibbs free energy profiles for reactions A4 and A5 at 1500 K and 3000 K. The reactant
408 (HtH-2) is labeled as "R". The transition state is labeled as "TS". The products are labeled as
409 "P".

410

411 **3. 2. 3. Product distribution**

412 The product evolution during the pyrolysis of HtH-1 and HtH-2 is tracked and
413 averaged from 10 independent simulations at each different temperature. The 10 species with
414 the highest concentration at the end of the simulation (0.5 ns) are shown at each temperature in
415 the supplementary material (S4). Figure 5 shows a comparison at 2000 K, where only
416 hydrocarbon species (> C_2) with more than 5 molecules (on average) existing at any given time,
417 termed major species, are plotted. Other (minor) species are not shown here, because their
418 concentrations are too small and are subject to large statistical uncertainties, which makes it

difficult to draw a clear trend from them. However, it should be noted that the list of major and minor species identified from the criteria can change over the simulation time and with temperatures, until the system reaches an equilibrium state. As discussed earlier, HtH-1 directly decomposes to two molecules of C_9H_{16} at 2000 K (reaction A1), therefore, its concentration initially increases quickly up to 0.05 ns. Since C_9H_{16} decomposition leads to the formation of C_5H_8 and C_4H_8 by unimolecular C-C bond fission, C_5H_8 and C_4H_8 keep increasing over the entire simulation time. Given that 23 C_9H_{16} molecules are still remaining at 0.5 ns (our simulation time), the number of C_5H_8 and C_4H_8 would continue to increase beyond this time. However, the detailed analysis with longer simulation time is not the aim of the current study. As shown in Fig. 5a, C_4H_8 is produced about twice as much as C_5H_8, indicating that there are other important pathways that produce C_4H_8. As shown in Table 3, HtH-1 decomposition produces $C_{14}H_{24}$ and C_4H_8 (reaction A2), and sequentially two pairs of products, $C_{10}H_{18}$ + C_4H_6 and C_8H_{14} + C_6H_{10} are produced from $C_{14}H_{24}$. Further unimolecular decomposition of $C_{10}H_{18}$ and C_8H_{14} leads to the formation of C_6H_{10} + C_4H_8 and C_4H_8 + C_4H_6, respectively.

In HtH-2 decomposition, $C_{12}H_{22}$, C_5H_{10}, C_4H_8, C_3H_6, and C_2H_4 are identified as major intermediates or products (Fig. 5b), and they are produced through various pathways. As shown in Table 3, $C_{17}H_{31}$ and CH_3 radicals are the major initial products from HtH-2 decomposition (reaction A5) at 2000 K, and $C_{17}H_{31}$ further breaks down to smaller fragments, such as $C_{16}H_{28}$ + CH_3, $C_{13}H_{23}$ + C_4H_8, $C_{12}H_{22}$ + C_5H_9, and $C_{12}H_{21}$ + C_5H_{10}, by unimolecular decomposition reactions. HtH-2 decomposition can be also initiated by reaction A4 which produces two C_9H_{17} radicals, and sequentially the C_9H_{17} radicals easily decompose to C_5H_9 + C_4H_8, C_7H_{13} + C_2H_4, and C_4H_7 + C_5H_{10}. The produced C_5H_9 and C_7H_{13} are further decomposed to C_2H_4 + C_3H_5, and C_3H_5 + C_4H_8 and C_3H_6 + C_4H_7, respectively. HtH-2 decomposition initiated by reaction A6 produces $C_{12}H_{22}$ and C_6H_{12}, and their further decomposition leads to the formation of $C_{11}H_{19}$ +

443 CH_3 and C_2H_4 + C_4H_8, respectively. The final decomposition route (reaction A7) generates
444 $C_{14}H_{26}$ and C_4H_8 as shown in Table 3, and $C_{14}H_{26}$ breaks down to $C_{12}H_{22}$ and C_2H_4.

445 One of the important fuel properties for aviation applications is the sooting tendency,
446 and the Yield Sooting Index (YSI) is a well-established and widely-used metric for sooting
447 tendency quantification based on soot yield [55, 56]. YSIs have been determined for HtH-1 and
448 HtH-2 to be 248 and 173, respectively, ([12]; details in the supplementary material S5), which
449 means that HtH-1 has a much higher tendency to form soot during combustion than HtH-2,
450 even though they have the same number of carbons. Our ReaxFF simulation results of the
451 product spectrum from HtH-1 and HtH-2 agree qualitatively with the experimentally measured
452 YSI trend. As shown in Fig. 5, major products from HtH-1 are C_5H_8 and C_4H_8, and those from
453 HtH-2 are C_4H_8 and C_2H_4. The unsaturated hydrocarbons are generally regarded as key soot
454 precursors leading to the formation of the first aromatic ring and consequently soot. However,
455 their effectiveness in forming soot is different. C_2H_4 is a relatively inefficient soot precursor,
456 because slow growth reactions are required to produce C3 species that are key species for
457 benzene formation [57-59]. In contrast, C_5H_8 and C_4H_8 are more effective soot precursors, since
458 they can produce not only C3 species by fast C-C fissions but also additional C1 or C2 species
459 [57, 60, 61]. Therefore, the ReaxFF results suggest that HtH-1 has a higher sooting tendency
460 than HtH-2, which is consistent with the experimental YSI trend for the two compounds.

461 Moreover, the ReaxFF pathways are consistent with the absolute sooting tendency of
462 HtH-1. The group-contribution method we developed earlier [55] predicts that YSI = 121.2 ±
463 14.7 for 1,5,5-trimethylcyclohexene (the C_9H_{16} isomer formed by (A1)). ReaxFF indicates that
464 at the temperatures where the fuel is consumed in the YSI flames – which is below 1500 K [62]
465 – the dominant process (> 81%; Table 3) is HtH-1 → 2 C_9H_{16}. Therefore, ReaxFF predicts that
466 the YSI of HtH-1 is ≈ 2 × 121 = 242, which agrees well with the measured value of 248.

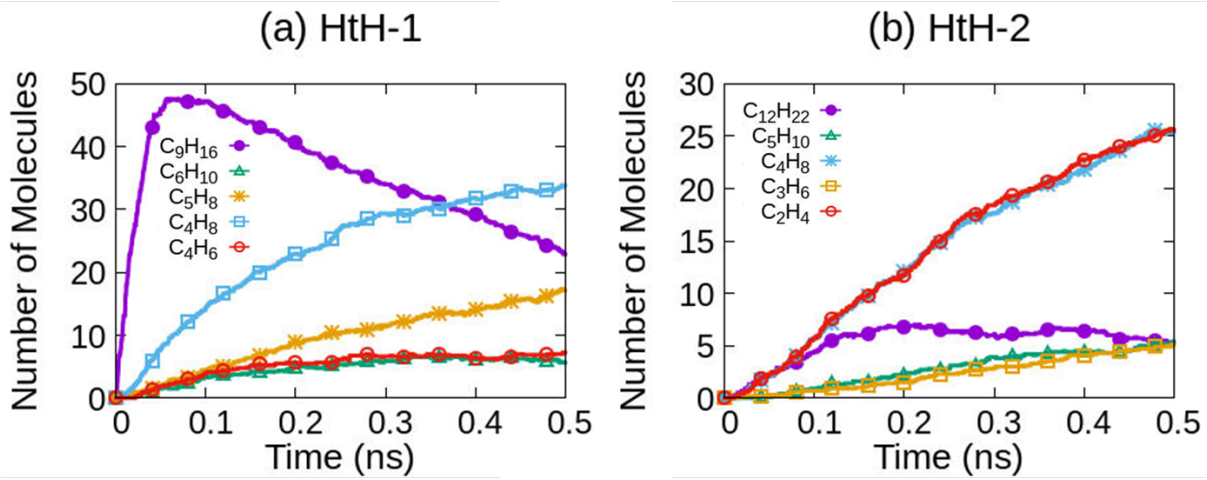

Fig. 5. Time evolution of the major products observed during the pyrolysis simulations of (a) HtH-1 and (b) HtH-2 at 2000 K. Results are averaged from 10 independent simulations. Only species with more than 5 molecules (on average) existing at any given time are plotted. For clarity, markers are only shown for every 400th data point.

3. 3. Pyrolysis of HtH-1 and HtH-2 mixtures

3. 3. 1. Decomposition rates

As mentioned in Section 1, the synthesis method by Ryan et al. [12] produced a mixture of 91.2 % HtH-1 (desired product) and 8.8 % HtH-2 (impurity). Given that the compounds are hard to separate, real jet fuels based on HtH-1 are likely to contain similar or higher levels of HtH-2. Therefore, this section investigates the impact of HtH-2 on pyrolysis of HtH-1 in three different mixture systems with mixing ratio α = 0.9, 0.7, and 0.5 as defined in Table 5. Since there are no significant density effects on the decomposition kinetics as shown in Fig. 2, these simulations are performed only with a density of 0.2 kg/dm^3. Figure 6 shows the global fuel decomposition rate constant plotted against the inverse of temperature, similar to Fig. 2. It is shown that the fitted straight lines shift downwards with decreasing mixing ratio of HtH-2,

indicating that the decomposition rate of the mixtures decreases when more HtH-2 molecules with less reactivity are added into the mixture. The effects of adding HtH-2 is more remarkable at lower temperatures, similar to previous ReaxFF results for other binary mixtures [22]. In single component systems, as shown in Fig. 2, the decomposition rate decreases more rapidly in HtH-2 than HtH-1 with decreasing temperature, which makes the fitted lines for HtH-1 and HtH-2 mixtures more divergent at lower temperatures in Fig. 6.

Based on the Arrhenius plot shown in Fig. 6, the activation energy and pre-exponential factor for the thermal decomposition of mixtures are calculated (using Eq. (2)) and shown in Table 5. The activation energy increases with higher fraction of HtH-2 in the mixture system, since HtH-2 (49.20 kcal/mol) has a higher activation energy than HtH-1 (27.97 kcal/mol) as shown in Table 2. The pre-exponential factor is about an order of magnitude higher for HtH-2 (5.99×10^{14} 1/s) than for HtH-1 (2.51×10^{13} 1/s) in single component systems, leading to an increase in pre-exponential factor when more HtH-2 is blended into the mixture.

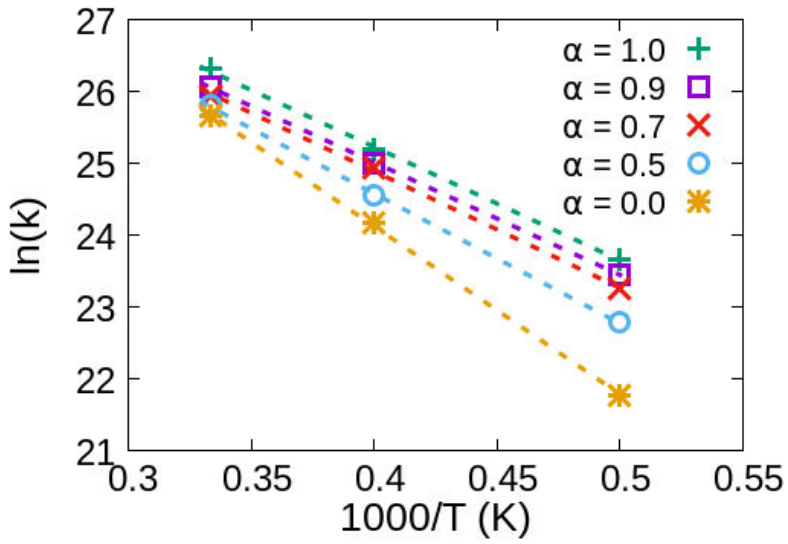

Fig. 6. The logarithm of the global reaction rate constant (k) plotted against the inverse of temperature (1000/T) in thermal decomposition of fuel mixtures with mixing ratio α = 1.0, 0.9, 0.7, 0.5, and 0.0 and a density of 0.2 kg/dm^3.

503 **Table 5.** Arrhenius parameters for thermal decomposition in HtH-1 and HtH-2 mixtures with
504 mixing ratio α = 0.9, 0.7, and 0.5. The Arrhenius parameters for HtH-1 (α = 1.0) and HtH-2 (α
505 = 0.0) in the single component systems are extracted from Table 2 and added for comparison.

Mixture ratio (α)	Mixture composition		E_a (kcal/mol)	A (1/s)
	HtH-1	HtH-2		
1.0	100%	-	27.97	2.51×10^{13}
0.9	90%	10%	31.12	3.84×10^{13}
0.7	70%	30%	32.25	4.26×10^{13}
0.5	50%	50%	35.96	6.60×10^{13}
0.0	-	100%	49.20	5.99×10^{14}

506

507 **3. 3. 2. Initial reaction mechanism**

508 To understand the underlying mechanism of the reduced decomposition rate by HtH-
509 2 blending, we plot the number of HtH-1 (or HtH-2) molecules normalized by the initial
510 number of HtH-1 (or HtH-2) molecules as a function of time in single component and mixture
511 systems. Figure 7(a) shows that the normalized number of HtH-1 over time has a very similar
512 behavior in all systems. These results suggest that the decomposition rate of mixtures is reduced
513 simply by the replacement of the more reactive HtH-1 by the less reactive HtH-2, but there is
514 no significant synergistic effect of HtH-2 addition on the initial thermal decomposition kinetics
515 of HtH-1. This conclusion is further confirmed by Fig. 7(b) which shows the normalized
516 number of HtH-2 in single component (α = 0) and mixture systems (α = 0.5 and 0.7). Since the
517 mixture system with α = 0.9 contains only 4 molecules of HtH-2, it is excluded from this
518 comparison. Figure 7(b) shows that HtH-2 decomposition kinetics is almost the same in all
519 cases, which indicates that HtH-1 and HtH-2 do not interact with each other in thermal
520 decomposition.

521

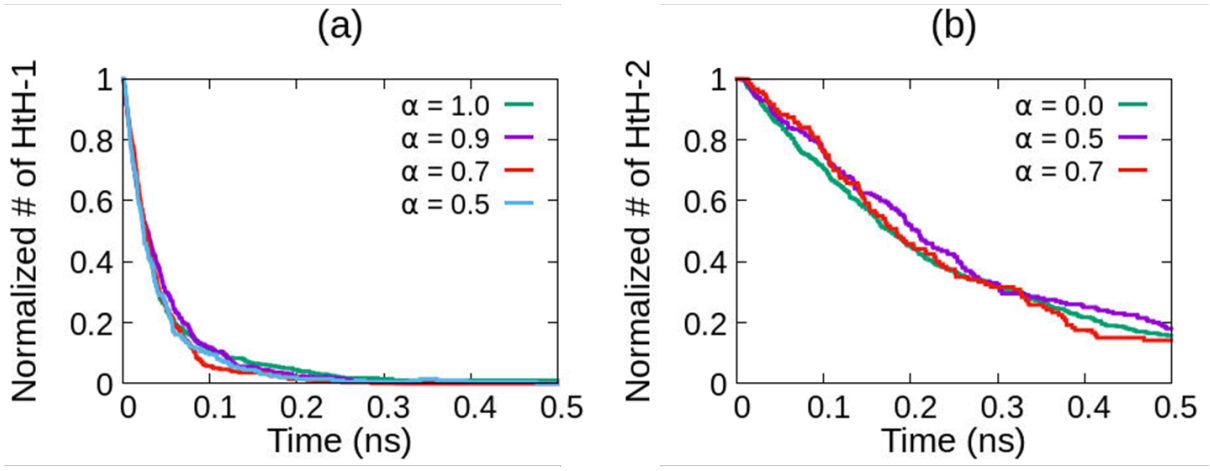

Fig. 7. Normalized number of (a) HtH-1 and (b) HtH-2 at 2000 K in single component and mixture systems. A mixing ratio of α = 1.0 corresponds to the single component HtH-1 case, and a mixing ratio of α = 0.0 corresponds to the single component HtH-2 case.

Next, the important initial reactions are identified in the three different mixtures using the same analysis described in Section 3. 2. 2. Table 6 shows the major initial reactions and their relative percentages observed in mixtures at 2000 K. Note that in each mixture system the relative percentages of reactions A1-A3 and reactions A4-A7 are calculated as the number of occurrences of these reactions normalized by the initial number of HtH-1 and HtH-2, respectively. In single component systems, A1-A3 and A4-A7 are the major initial reactions observed in the decomposition of HtH-1 and HtH-2, respectively, and they are still the most important reactions in mixture systems. In addition, Table 6 shows that the relative percentages of reactions A1-A7 stay almost the same for all three mixing ratios. These results indicate that there is no significant interaction between HtH-1 and HtH-2 during their thermal decomposition, since each fuel is primarily decomposed by unimolecular reactions. Although here we only show the results at 2000 K, the same conclusion is also observed at different temperatures.

Table 6. Initial decomposition reaction channels in fuel mixtures at 2000K.

Reactant	Initial Products	Percentage		
		α = 0.9	α = 0.7	α = 0.5
HtH-1 ($C_{18}H_{32}$)	(A1) $C_9H_{16} + C_9H_{16}$	64%	68%	66%
	(A2) $C_{14}H_{28} + C_4H_8$	20%	16%	16%
	(A3) $C_{17}H_{29} + CH_3$	4%	4%	5%
HtH-2 ($C_{18}H_{34}$)	(A4) $C_9H_{17} + C_9H_{17}$	20%	19%	18%
	(A5) $C_{17}H_{31} + CH_3$	26%	31%	33%
	(A6) $C_{12}H_{22} + C_6H_{12}$	9%	14%	10%
	(A7) $C_{14}H_{26} + C_4H_8$	20%	10%	10%

3. 3. 3. Product distribution

This section investigates whether the addition of HtH-2 affects the major product evolution for the pyrolysis of fuel mixtures. We plot the number of C_9H_{16}, C_6H_{10}, C_5H_8, and C_4H_6 molecules normalized by the initial number of HtH-1 molecules in the single component system (α = 1.0) and mixture systems (α = 0.9, 0.7, and 0.5). The four species are selected since they are the main products derived from HtH-1 decomposition. Figure 8 shows that the time history of the normalized numbers of product molecules are very similar although HtH-2 is added up to 50% in the mixture system. These results demonstrate that decomposition of the HtH-1 derived species occurs via unimolecular reactions, and is hardly affected by HtH-2 or the HtH-2 derived species. However, it should be noted that further decomposition or growth reactions of the HtH-1 products over longer time-scales might be influenced by the presence of HtH-2 derived products, because it would provide different intermediates or radicals which will potentially participate in bimolecular reactions. However, this is outside the scope of the current work.

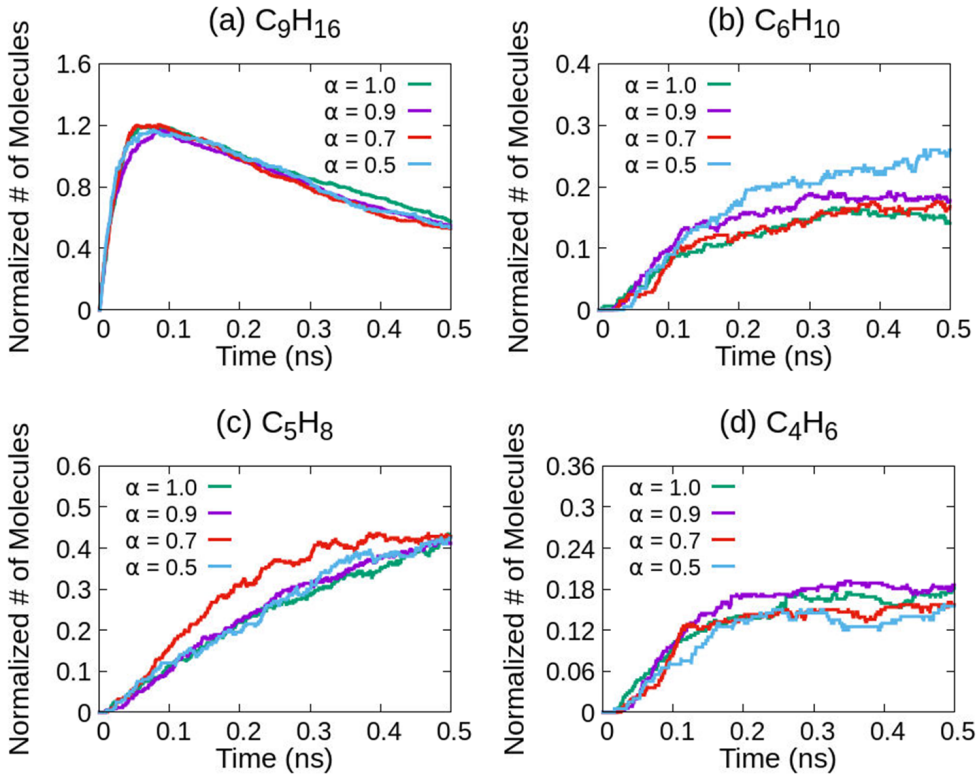

Fig. 8. Number of product molecules derived from HtH-1, including (a) C_9H_{16}, (b) C_6H_{10}, (c) C_5H_8, and (d) C_4H_6, in single component system (α = 1.0) and mixture systems (α = 0.9, 0.7, and 0.5). Profiles are normalized by the initial number of HtH-1 molecules in the system.

4. Conclusions

The initial pyrolysis chemistry for HtH-1, a potential fuel candidate for aviation applications, and HtH-2, which acts as an impurity produced by fuel synthesis, was investigated in this work using ReaxFF based molecular dynamics (MD) simulations. The bond dissociation energies (BDE) for important bonds were calculated using both ReaxFF and density function theory (DFT) calculations to provide insight into fuel decomposition via unimolecular reactions and to validate the force field employed in the study. ReaxFF-MD simulations were performed at different densities (0.1 kg/dm^3, 0.2 kg/dm^3, and 0.3 kg/dm^3) and temperatures (1500 K, 1800 K, 2000 K, 2500 K, and 3000 K) to investigate the initial decomposition kinetics and decomposition mechanism during the pyrolysis of HtH-1 and HtH-2.

573 Global Arrhenius parameters, such as activation energies and pre-exponential factors,
574 were calculated, and used to analyze the overall decomposition kinetics of the fuels. It was
575 found that HtH-1 has a faster decomposition rate than HtH-2, and both fuels have higher
576 reactivity compared to several existing jet-fuel components, such as JP-10, *n*-dodecane, *iso*-
577 octane, and toluene. A temperature-dependent initial decomposition mechanism was also
578 elucidated using a systematic reaction analysis framework developed in this work. It was
579 shown that the central C-C bond connecting the two cyclohexane rings preferentially
580 decomposes at lower temperature in both HtH-1 and HtH-2 fuels. However, initial
581 decomposition via C-CH_3 bond breaking becomes important with increasing temperature due
582 to the large increase in entropy during this reaction. We also identified the product distribution
583 during the pyrolysis process. HtH-1 mostly produces C_5H_8 and C_4H_8, while HtH-2 produces
584 C_4H_8 and C_2H_4. These results were consistent with the higher sooting tendency of HtH-1 than
585 HtH-2 observed in experimental measurements. To investigate the effects of HtH-2 on the
586 pyrolysis behavior of HtH-1, the same analyses were also performed in their binary fuel
587 mixtures. The ReaxFF results demonstrated that HtH-1 and HtH-2 decompose by unimolecular
588 reactions, and there is no significant interaction between the two fuels during the pyrolysis of
589 the mixtures.
590 It is worth reemphasizing that the analysis performed using ReaxFF offers a reliable
591 way to investigate hydrocarbon fuel chemistry at a fraction of the computational cost of the
592 equivalent DFT calculations without any *a priori* input and chemical intuition. The ReaxFF-
593 based systematic reaction analysis shown in this work can be used as a standard framework to
594 understand pyrolysis and combustion chemistry of existing or future fuels and to contribute to
595 the development of their chemical kinetic models.
596
597

Acknowledgments

This research was funded by the U.S. Department of Energy's Office of Energy Efficiency and Renewable Energy (EERE) under the Bioenergy Technologies Office (BETO) and Vehicle Technologies Office (VTO) Program Award Number DE-EE0007983. AL and ACTvD also acknowledge funding from AFOSR grant FA9550-17-1-0173.

References

[1] Wei H, Liu W, Chen X, Yang Q, Li J, Chen H. Renewable bio-jet fuel production for aviation: A review. Fuel 2019;254:115599.

[2] Kandaramath Hari T, Yaakob Z, Binitha NN. Aviation biofuel from renewable resources: Routes, opportunities and challenges. Renewable and Sustainable Energy Reviews 2015;42:1234-44.

[3] Gutiérrez-Antonio C, Gómez-Castro FI, de Lira-Flores JA, Hernández S. A review on the production processes of renewable jet fuel. Renewable and Sustainable Energy Reviews 2017;79:709-29.

[4] Chiaramonti D, Prussi M, Buffi M, Tacconi D. Sustainable bio kerosene: Process routes and industrial demonstration activities in aviation biofuels. Applied Energy 2014;136:767-74.

[5] Kosir ST, Behnke L, Heyne JS, Stachler RD, Flora G, Zabarnick S, et al. Improvement in jet aircraft operation with the use of high-performance drop-in fuels. AIAA Scitech 2019 Forum. American Institute of Aeronautics and Astronautics; 2019.

[6] Holladay J, Abdullah Z, Heyne J. Sustainable aviation fuel: Synthesized recommendations from three workshops. Pacific Northwest National Laboratories 2019;PNNL-28815.

[7] Zhang X, Pan L, Wang L, Zou J-J. Review on synthesis and properties of high-energy-density liquid fuels: Hydrocarbons, nanofluids and energetic ionic liquids. Chem Eng Sci 2018;180:95-125.

[8] Chung HS, Chen CSH, Kremer RA, Boulton JR, Burdette GW. Recent developments in high-energy density liquid hydrocarbon fuels. Energy Fuels 1999;13(3):641-9.

[9] Tang H, Li N, Li S, Chen F, Li G, Wang A, et al. Synthesis of jet fuel rang cycloalkane from isophorone with glycerol as a renewable hydrogen source. Catal Today 2017;298:16-20.
[10] Wang W, Liu Y, Li N, Li G, Wang W, Wang A, et al. Synthesis of renewable high-density fuel with isophorone. Scientific Reports 2017;7(1):6111.
[11] Xie J, Zhang L, Zhang X, Han P, Xie J, Pan L, et al. Synthesis of high-density and low-freezing-point jet fuel using lignocellulose-derived isophorone and furanic aldehydes. Sustainable Energy & Fuels 2018;2(8):1863-9.
[12] Ryan CF, Moore CM, Leal JH, Semelsberger TA, Banh JK, Zhu J, et al. Synthesis of aviation fuel from bio-derived isophorone. Sustainable Energy & Fuels 2020;4(3):1088-92.
[13] Billaud F, Chaverot P, Berthelin M, Freund E. Thermal decomposition of cyclohexane at approximately 810.degree.C. Industrial & Engineering Chemistry Research 1988;27(5):759-64.
[14] Kim J, Park SH, Lee CH, Chun B-H, Han JS, Jeong BH, et al. Coke formation during thermal decomposition of methylcyclohexane by alkyl substituted C_5 ring hydrocarbons under supercritical conditions. Energy Fuels 2012;26(8):5121-34.
[15] Dai Y, Zhao W, Xie H, Guo Y, Fang W. Pyrolysis kinetics and mechanism of ethylcyclohexane. J Anal Appl Pyrolysis 2020;145:104723.
[16] Gough RV, Widegren JA, Bruno TJ. Thermal decomposition kinetics of 1,3,5-triisopropylcyclohexane. Industrial & Engineering Chemistry Research 2013;52(24):8200-5.
[17] Yu J, Eser S. Thermal decomposition of jet fuel model compounds under near-critical and supercritical conditions. 1. n-butylbenzene and n-butylcyclohexane. Industrial & Engineering Chemistry Research 1998;37(12):4591-600.
[18] Yu J, Eser S. Thermal decomposition of jet fuel model compounds under near-critical and supercritical conditions. 2. decalin and tetralin. Industrial & Engineering Chemistry Research 1998;37(12):4601-8.
[19] Chae K, Violi A. Thermal decomposition of decalin: An ab initio study. The Journal of Organic Chemistry 2007;72(9):3179-85.
[20] Xing Y, Fang W, Xie W, Guo Y, Lin R. Thermal cracking of JP-10 under pressure. Industrial & Engineering Chemistry Research 2008;47(24):10034-40.

[21] Chenoweth K, van Duin ACT, Dasgupta S, Goddard Iii WA. Initiation mechanisms and kinetics of pyrolysis and combustion of JP-10 hydrocarbon jet fuel. J Phys Chem A 2009;113(9):1740-6.
[22] Ashraf C, Shabnam S, Jain A, Xuan Y, van Duin ACT. Pyrolysis of binary fuel mixtures at supercritical conditions: A ReaxFF molecular dynamics study. Fuel 2019;235:194-207.
[23] Gao CW, Vandeputte AG, Yee NW, Green WH, Bonomi RE, Magoon GR, et al. JP-10 combustion studied with shock tube experiments and modeled with automatic reaction mechanism generation. Combust Flame 2015;162(8):3115-29.
[24] Yue L, Qin X, Wu X, Guo Y, Xu L, Xie H, et al. Thermal decomposition kinetics and mechanism of 1,1′-bicyclohexyl. Energy Fuels 2014;28(7):4523-31.
[25] Curran HJ. Developing detailed chemical kinetic mechanisms for fuel combustion. Proc Combust Inst 2019;37(1):57-81.
[26] van Duin ACT, Dasgupta S, Lorant F, Goddard WA. ReaxFF: A reactive force field for hydrocarbons. J Phys Chem A 2001;105(41):9396-409.
[27] Chenoweth K, van Duin ACT, Goddard WA. ReaxFF reactive force field for molecular dynamics simulations of hydrocarbon oxidation. J Phys Chem A 2008;112(5):1040-53.
[28] Senftle TP, Hong S, Islam MM, Kylasa SB, Zheng Y, Shin YK, et al. The ReaxFF reactive force-field: development, applications and future directions. Npj Comput Mater 2016;2:15011.
[29] Mortier WJ, Ghosh SK, Shankar S. Electronegativity-equalization method for the calculation of atomic charges in molecules. J Am Chem Soc 1986;108(15):4315-20.
[30] Castro-Marcano F, van Duin ACT. Comparison of thermal and catalytic cracking of 1-heptene from ReaxFF reactive molecular dynamics simulations. Combust Flame 2013;160(4):766-75.
[31] Wang Q-D, Wang J-B, Li J-Q, Tan N-X, Li X-Y. Reactive molecular dynamics simulation and chemical kinetic modeling of pyrolysis and combustion of n-dodecane. Combust Flame 2011;158(2):217-26.
[32] Cheng X-M, Wang Q-D, Li J-Q, Wang J-B, Li X-Y. ReaxFF molecular dynamics simulations of oxidation of toluene at high temperatures. J Phys Chem A 2012;116(40):9811-8.

690 [33] Liu L, Bai C, Sun H, Goddard WA. Mechanism and Kinetics for the Initial Steps of
691 Pyrolysis and Combustion of 1,6-Dicyclopropane-2,4-hexyne from ReaxFF Reactive
692 Dynamics. J Phys Chem A 2011;115(19):4941-50.
693 [34] Han S, Li X, Zheng M, Guo L. Initial reactivity differences between a 3-component
694 surrogate model and a 24-component model for RP-1 fuel pyrolysis evaluated by ReaxFF
695 MD. Fuel 2018;222:753-65.
696 [35] Zhao P, Han S, Li X, Zhu T, Tao X, Guo L. Comparison of RP-3 Pyrolysis Reactions
697 between Surrogates and 45-Component Model by ReaxFF Molecular Dynamics
698 Simulations. Energy Fuels 2019;33(8):7176-87.
699 [36] Liu X, Li X, Nie F, Guo L. Initial Reaction Mechanism of Bio-oil High-Temperature
700 Oxidation Simulated with Reactive Force Field Molecular Dynamics. Energy Fuels
701 2017;31(2):1608-19.
702 [37] Mayo SL, Olafson BD, Goddard WA. DREIDING: a generic force field for
703 molecular simulations. J Phys Chem 1990;94(26):8897-909.
704 [38] Ashraf C, van Duin ACT. Extension of the ReaxFF combustion force field toward
705 syngas combustion and initial oxidation kinetics. J Phys Chem A 2017;121(5):1051-68.
706 [39] Arvelos S, Abrahão O, Eponina Hori C. ReaxFF molecular dynamics study on the
707 pyrolysis process of cyclohexanone. J Anal Appl Pyrolysis 2019;141:104620.
708 [40] Kwon H, Shabnam S, van Duin ACT, Xuan Y. Numerical simulations of yield-based
709 sooting tendencies of aromatic fuels using ReaxFF molecular dynamics. Fuel
710 2019;262(15):116545.
711 [41] Feng M, Jiang XZ, Mao Q, Luo KH, Hellier P. Initiation mechanisms of enhanced
712 pyrolysis and oxidation of JP-10 (exo-tetrahydrodicyclopentadiene) on functionalized
713 graphene sheets: Insights from ReaxFF molecular dynamics simulations. Fuel
714 2019;254:115643.
715 [42] Chen Z, Sun W, Zhao L. Combustion mechanisms and kinetics of fuel additives: A
716 ReaxFF molecular simulation. Energy Fuels 2018;32(11):11852-63.
717 [43] Chen Z, Sun W, Zhao L. Initial mechanism and kinetics of diesel incomplete
718 combustion: ReaxFF molecular dynamics based on a multicomponent fuel model. The
719 Journal of Physical Chemistry C 2019;123(14):8512-21.
720 [44] Berendsen HJC, Postma JPM, van Gunsteren WF, DiNola A, Haak JR. Molecular
721 dynamics with coupling to an external bath. J Chem Phys 1984;81(8):3684-90.

[45] Bal KM, Neyts EC. Merging metadynamics into hyperdynamics: Accelerated molecular simulations reaching time scales from microseconds to seconds. Journal of Chemical Theory and Computation 2015;11(10):4545-54.
[46] Bal KM, Neyts EC. Direct observation of realistic-temperature fuel combustion mechanisms in atomistic simulations. Chemical Science 2016;7(8):5280-6.
[47] te Velde G, Bickelhaupt FM, Baerends EJ, Fonseca Guerra C, van Gisbergen SJA, Snijders JG, et al. Chemistry with ADF. J Comput Chem 2001;22(9):931-67.
[48] Kiefer JH, Gupte KS, Harding LB, Klippenstein SJ. Shock tube and theory investigation of cyclohexane and 1-hexene decomposition. J Phys Chem A 2009;113(48):13570-83.
[49] Bochevarov AD, Harder E, Hughes TF, Greenwood JR, Braden DA, Philipp DM, et al. Jaguar: A high-performance quantum chemistry software program with strengths in life and materials sciences. Int J Quantum Chem 2013;113(18):2110-42.
[50] Becke AD. Density-functional thermochemistry. III. The role of exact exchange. J Chem Phys 1993;98(7):5648-52.
[51] Krishnan R, Binkley JS, Seeger R, Pople JA. Self-consistent molecular orbital methods. XX. A basis set for correlated wave functions. J Chem Phys 1980;72(1):650-4.
[52] Csonka GI, Ruzsinszky A, Tao J, Perdew JP. Energies of organic molecules and atoms in density functional theory. Int J Quantum Chem 2005;101(5):506-11.
[53] Nachtigall P, Sauer J. Chapter 20 - Applications of quantum chemical methods in zeolite science. In: Čejka J, van Bekkum H, Corma A, Schüth F, editors. Studies in Surface Science and Catalysis. Elsevier; 2007, p. 701-XXI.
[54] Wang E, Ding J, Qu Z, Han K. Development of a reactive force field for hydrocarbons and application to iso-octane thermal decomposition. Energy Fuels 2018;32(1):901-7.
[55] Das DD, St. John PC, McEnally CS, Kim S, Pfefferle LD. Measuring and predicting sooting tendencies of oxygenates, alkanes, alkenes, cycloalkanes, and aromatics on a unified scale. Combust Flame 2018;190:349-64.
[56] McEnally CS, Das DD, Pfefferle LD. Yield sooting index database volume 2: Sooting tendencies of a wide range of fuel compounds on a unified scale. Harvard Dataverse, V1 2017.

[57] McEnally CS, Pfefferle LD, Atakan B, Kohse-Höinghaus K. Studies of aromatic hydrocarbon formation mechanisms in flames: Progress towards closing the fuel gap. Prog Energy Combust Sci 2006;32(3):247-94.
[58] McEnally CS, Ciuparu DM, Pfefferle LD. Experimental study of fuel decomposition and hydrocarbon growth processes for practical fuel components: heptanes. Combust Flame 2003;134(4):339-53.
[59] Kwon H, Etz BD, Montgomery MJ, Messerly R, Shabnam S, Vyas S, et al. Reactive Molecular Dynamics Simulations and Quantum Chemistry Calculations To Investigate Soot-Relevant Reaction Pathways for Hexylamine Isomers. J Phys Chem A 2020;124(21):4290-304.
[60] McEnally CS, Pfefferle LD. Fuel decomposition and hydrocarbon growth processes for oxygenated hydrocarbons: butyl alcohols. Proc Combust Inst 2005;30(1):1363-70.
[61] Jin H, Wang G, Wang Y, Zhang X, Li Y, Zhou Z, et al. Experimental and kinetic modeling study of laminar coflow diffusion methane flames doped with iso-butanol. Proc Combust Inst 2017;36(1):1259-67.
[62] McEnally CS, Xuan Y, St. John PC, Das DD, Jain A, Kim S, et al. Sooting tendencies of co-optima test gasolines and their surrogates. Proc Combust Inst 2019;37(1):961-8.